

TRAF-interacting protein with forkhead-associated domain (TIFA) transduces DNA damage-induced activation of NF- κ B

Jingxuan Fu^{1,2}, Daoyuan Huang^{1,2}, Fuwen Yuan^{1,2}, Nan Xie^{1,2}, Qian Li³, Xinpei Sun^{1,2},
Xuehong Zhou², Guodong Li^{1,2}, Tanjun Tong^{1,2*} and Yu Zhang^{1,2*}

¹Peking University Research Center on Aging, Peking University Health Science Center, Beijing 100191, People's Republic of China; ²Department of Biochemistry and Molecular Biology, School of Basic Medical Sciences, Peking University Health Science Center, Beijing 100191, People's Republic of China; ³Department of Orthodontics, Peking University School and Hospital of Stomatology, National Engineering Laboratory for Digital and Material Technology of Stomatology, Beijing Key Laboratory of Digital Stomatology, Beijing 100081, People's Republic of China

Running title: *TIFA promotes DNA damage-induced NF- κ B activation*

*To whom correspondence should be addressed: Yu Zhang, Department of Biochemistry and Molecular Biology, Peking University Health Science Center, 38 Xue Yuan Road, Beijing 100191, China, Telephone: 86-10-82805661. Email: zhang_yu@hsc.pku.edu.cn or Tanjun Tong, Department of Biochemistry and Molecular Biology, Peking University Health Science Center, 38 Xue Yuan Road, Beijing 100191, China, Telephone: 86-10-82801454, Fax: 86-10-82802931. Email: ttj@bjmu.edu.cn

Keywords: DNA damage, nuclear factor kappa B transcription factor, ubiquitination, carcinogenesis, TRAF, NEMO, TIFA, TRAF-interacting protein with forkhead-associated domain

ABSTRACT

DNA damage-induced NF- κ B activation and the secretion of inflammatory cytokines play crucial roles in carcinogenesis and cellular senescence. However, the underlying mechanisms, especially the initial sensors and transducers connecting the nuclear DNA damage signal with cytoplasmic NF- κ B activation remain incompletely understood. Here, we report that TRAF-interacting protein with forkhead-associated domain (TIFA), an established NF- κ B activator in the cytosol, unexpectedly exhibited nuclear translocation and accumulation on damaged chromatin following genotoxic stress.

Accordingly, we also found that DNA damage-induced transcriptional activation and the resulting secretion of classic NF- κ B targets, including interleukin (IL)-6 and IL-8, was greatly enhanced in TIFA-overexpressing cells compared with control cells. Mechanistically, DNA damage induced TIFA phosphorylation at threonine 9 (pThr-9), and this phosphorylation event, involving the pThr-binding forkhead-associated domain, was crucial for its enrichment on damaged chromatin and subsequent NF- κ B activation. Moreover, in conjunction with its partner protein, the E3 ligase TNF receptor-associated factor 2 (TRAF2), TIFA relayed the DNA damage

signals by stimulating ubiquitination of NF- κ B essential modulator (NEMO), whose sumoylation, phosphorylation and ubiquitination were critical for NF- κ B's response to DNA damage. Consistently, TRAF2 knockdown suppressed TIFA overexpression-enhanced NEMO ubiquitination under genotoxic stress, and a unphosphorylatable Thr-9-mutated TIFA variant had only minor effects on NEMO polyubiquitination. Finally, in agreement with the model of DNA damage-associated secretory senescence barrier against carcinogenesis, ectopic TIFA expression limited proliferation of multiple myeloma cancer cells. In conclusion our results indicate that TIFA functions as a key transducer in DNA damage-induced NF- κ B activation.

INTRODUCTION

Genomic instability and associated DNA damage response (DDR) are common hallmarks in cancer and aging (1). An emerging theme in DDR induced cellular phenotypic change is the dramatically increased secretion of myriad inflammatory factors, including cytokines, chemokines and interferons, which contribute to cancer development and senescence progression in autocrine, paracrine or endocrine fashions via their collaborations with DDR (1). Such secretome alternations are manifested in the conditions with oncogene overexpression or tumor suppressor inactivation, and hence are designated as "senescence-associated secretory phenotype" (SASP) in the senescence barrier model of malignancy (2).

The nuclear factor- κ B (NF- κ B) family transcription factors are master regulators for transcriptional activation of secretory factors, especially during cellular response

to the genotoxic stress (3). Despite the diversity of upstream stimuli, the NF- κ B cascade shares a common activation scheme consisting of phosphorylation, ubiquitination, and degradation of I κ B (inhibitors of NF- κ B) proteins, which result in the nuclear translocation of NF- κ B with masked nuclear localization signal of I κ B exposed (4). A plethora of physical and chemical stresses engage specific receptors and intracellular adaptors to transduce signals, and they generally converge on the activation of I κ B-kinase complex (IKK), which is composed by the catalytic subunit (IKK α or IKK β) and the regulatory subunit (IKK γ , also known as NEMO) (4). TRAF (TNF receptor associated factor)-family proteins, represented by TRAF2 and TRAF6 with a N-terminal RING finger domain, are key intermediates in many NF- κ B signaling pathways, employing their E3 ligase activity to synthesize a regulatory lysine 63-linked polyubiquitin chain on target proteins (4,5). The K63-linked polyubiquitin chain, critical for the assembly of TAK1-TAB2/TAB3 and IKK complexes, is directly bound by ubiquitin recognizing modules from TABs or NEMO, and the TAK1-TAB2/TAB3 complex could subsequently trigger IKK phosphorylation and activation (5).

The "inside-out" transduction of DNA damage signals obliges nucleocytoplasmic shuttling mechanisms, and NEMO exploits its post-translational modifications to meet this requirement and hence takes a center stage in DNA damage-induced NF- κ B activation (3,6). Following genotoxic stress, NEMO in the nucleus is sequentially modified with sumoylation, phosphorylation, and ubiquitination (7). Sumoylation of wild-type NEMO promotes its nuclear localization, while the non-sumoylatable NEMO is almost exclusively retained in

cytoplasm and deficient for NF- κ B activation following DNA damage (3,7). The necessity of NEMO phosphorylation was demonstrated by the failure of serine 85 to alanine mutant of NEMO for monoubiquitination and subsequent nuclear transport (8). NEMO monoubiquitination occurs on the same lysine (277 and 309) as sumoylation, but functionally counteracts with the nuclear localization preference caused by sumoylation, thereby contributes to the propagation of DNA damage signals outside of nucleus and to the ultimate IKK activation taking place in cytoplasm (3,7).

In early two-hybrid screening with TRAF2 or TRAF6 used as bait, TRAF-interacting protein with forkhead-associated domain (TIFA) was firstly identified as a TRAF-interacting protein (9,10). It contains a characteristic forkhead-associated (FHA) domain, which specifically binds to phosphorylated threonine (11). FHA domain is intimately linked to DNA damage-repair pathways due to the prevalence of phosphorylation events in multiprotein complex assembly following genotoxic stress, and such significance could be demonstrated by several FHA-containing proteins, such as MDC1, NBS1 and CHK1 in DDR and cell cycle checkpoint activation (12). Along with the critical function of TRAF in NF- κ B cascade, TIFA was reported to participate in canonical NF- κ B signaling pathway by promoting oligomerization and ubiquitination of TRAF proteins (13). Interestingly, under tumor necrosis factor alpha (TNF- α) stimulation, TIFA is phosphorylated at threonine 9, which could be recognized by its FHA domain. The resultant intermolecular binding between FHA and threonine phosphorylation leads to TIFA

oligomerization and TIFA-mediated NF- κ B activation (14).

Here, with our long term interest in the interface between carcinogenesis and aging (15-21), we focused on the molecular mechanisms of DNA damage-induced NF- κ B activation and secretion in this study. We identified TIFA as a novel regulator for this pathway and delineated the biochemical mechanisms underlying TIFA/TRAF2 complex mediated NF- κ B activation following genotoxic stress.

RESULTS

Enrichment of TIFA on Chromatin Following DNA Damage

In an attempt to identify novel adaptors of DNA damage-induced NF- κ B activation, we screened a panel of candidates from known NF- κ B activators. We first monitored their localization following DNA damage, reasoning that initial sensors of genotoxic stress should be enriched in nucleus. Microscopic examination using FLAG-fused proteins revealed an established NF- κ B regulator, TIFA, which was reported to be cytosolic under IL-1 and TNF stimulation (9), showed significant nuclear translocations and partial co-localization with γ H2AX following etoposide (ETO) treatment (Fig. 1A). This observation was independently supported with biochemical fractionation experiment using chromatins isolated from HeLa cells, as the loading of FLAG-tagged TIFA onto chromatin in ETO-treated cells was evident along with DNA damage-induced γ H2AX enrichment compared with control cells (Fig. 1B). Another fractionation approach with nuclear lysis buffer containing 150 mM KOAc (22) further confirmed that TIFA could be loaded onto damaged chromatin, with a corresponding decrease in cytoplasm

(Fig. 1C). Moreover, TIFA enrichment on chromatin was not observed following LPS treatment, indicating translocation of TIFA is specific to DNA damage treatment (Fig. 1D).

To better understand the function of TIFA, we generated an antibody against TIFA with high specificity (Fig. S1). We then consolidated DNA damage-induced TIFA enrichment on chromatin using this antibody and a pair of multiple myeloma cell lines (see below). The U266 cell lines with low endogenous TIFA expression was stably integrated with TIFA expression cassette and the chromatin fractionation results confirmed the concomitant enrichment of TIFA and γ H2AX when treated with ETO (Fig. 1E). Importantly, although the RPMI-8226 cells bearing high endogenous TIFA expression showed chromatin-bound TIFA in the resting state correlating with their higher level of spontaneous DNA damages, the ETO treatment caused increased TIFA loading onto chromatin, implying DNA damage induced TIFA dynamics in *in vivo* settings (Fig. 1F).

TIFA Potentiates DNA Damage-induced NF- κ B Activation and Secretion

Although the implications of TIFA in canonical NF- κ B pathways have been studied, there have been no reports on the role of TIFA in DNA damage-induced NF- κ B activation, to our knowledge. Given the novel observations on nuclear translocation and chromatin accumulation of TIFA following DDR, we then examined NF- κ B activation in DNA damage conditions with a gain-of-function model for TIFA.

We firstly performed luciferase reporter assay using the reporter construct with a classic NF- κ B binding motif. In this experiment, the reporter was strongly activated in HeLa cells stably transfected with TIFA expression vector 6 h after ETO treatment, but such activation was barely detected in the control cells (Fig. 2A). Importantly, the critical event in NF- κ B activation indicated by I κ B α phosphorylation could only be observed in TIFA-transfected cells following ETO treatment (Fig. 2B). We then measured the mRNA expression level changes for three classic NF- κ B targets, including *IL-6*, *IL-8* and *A20*, following DNA damage and TIFA overexpression. Using quantitative RT-PCR, we found all the three genes were up-regulated after ETO treatment in the TIFA-overexpressed HeLa cells but not in their control cells (Fig. 2C). Quantitative assessment of IL-6 and IL-8 secretion levels using enzyme-linked immunosorbent assays (ELISA) further supported TIFA-promoted NF- κ B activation following DDR, as the secretion of these two cytokines in TIFA-overexpressed cells relative to control cells was significantly increased when the cells were exposed to ETO (Fig. 2D).

The Significance of Phosphorylation Event in TIFA-mediated NF- κ B Activation

With the fact that TIFA could be accumulated on damaged DNA (Fig. 1) and the significance of FHA domain in DDR signaling pathways, it would be interesting to test the function of FHA domain on TIFA-mediated NF- κ B activation. Indeed, two groups of point mutations in the conserved residues of FHA domain (MT1, R51A/K88A/N89A or MT2, G50E/S66A) (10,14), abolished TIFA-mediated transcriptional activation of *IL-6* and *IL-8*

following ETO treatment. On the other hand, the sole FHA domain of TIFA also failed to induce *IL-6* and *IL-8* transcription (Fig. 3A).

To understand the molecular basis for DNA damage-induced chromatin accumulation of TIFA, we first performed co-immunoprecipitation assay to test the physical association between TIFA and γ H2AX, given the pivotal role of γ H2AX in marking DNA damage and orchestrating numerous signaling pathways in DDR. The results indicated that the interaction between TIFA and γ H2AX was increased upon ETO treatment, while the immunoprecipitation efficiency using FLAG antibody was comparable in control versus damage conditions (Fig. 3B). This point was further supported by the epistasis test using cells co-transfected with TIFA and H2AX mutants (S139A or S139E). Quantitative RT-PCR results suggested that co-transfection of the phosphorylation mimicking mutant S139E of H2AX showed greater activation of *IL-8* and *A20*, while the non-phosphorylatable mutant S139A of H2AX suppressed TIFA's effect (Fig. 3C). These functional interactions could only be observed under DNA damage conditions but not in LPS-treated cells, implying the specific dependence of TIFA on H2AX in DNA damage-induced NF- κ B activation.

The direct intermolecular association between FHA domain and the phosphothreonine (pThr9) (14,23) prompted us to test whether pThr9 was implicated in TIFA activation following genotoxic stress. Surprisingly, the single point mutation at Thr9 (TIFA-T9A) was sufficient to abolish its enrichment on damaged chromatin (Fig. 3D). Consistent with this result, TIFA-T9A showed minimal effect on DNA damage-induced NF- κ B activation

evidenced by decreased I κ B α phosphorylation, sustained total I κ B α protein levels (Fig. 3E) and blunted up-regulation of NF- κ B targets (Fig. 3F) in TIFA-T9A transfected cells compared to the wild-type TIFA transfected cells. Examination of phosphorylation state of TIFA suggested that DNA damage could effectively induce its phosphorylation (Fig. 3G). Importantly, such phosphorylation event could not be detected by use of TIFA-T9A, indicating DNA damage-elicited TIFA phosphorylation occurred at Thr9 (Fig. 3G). These data collectively suggested that TIFA engages phosphorylation-triggered intermolecular FHA binding to propagate DNA damage signals to NF- κ B.

TIFA Potentiates DNA Damage-induced NF- κ B Activation in Myeloma Cells

In order to understand the molecular function of endogenous TIFA in genotoxic stress-induced NF- κ B activation, we then surveyed the Cancer Cell Line Encyclopedia datasets with published mRNA profiles across over 1000 cell lines for TIFA expression patterns (24). We found TIFA was highly expressed in haematopoietic or lymphoid cell lines (Fig. 4A). With the antibody capable of efficiently probing endogenous TIFA proteins, we confirmed the high levels of TIFA in NALM-6 and RPMI-8226, both were B cell derived cancer cell lines (Fig. 4B). As a control, TIFA was lowly expressed in U266 cells. Consistent with the data in TIFA-stably expressed HeLa cells, overexpression of TIFA in U266 cell lines using lentivirus caused efficient I κ B α and IKK phosphorylation and significant up-regulation of *IL-6* and *IL-8* following ETO treatment (Fig. 4C, 4D and 4E). To further explore TIFA-associated secretory

changes, we screened a panel of SASP factors identified previously (2), and found the mRNA expression levels of *IL-11*, *CCL5*, *CXCL3*, *CXCL10*, *GM-CSF*, *MCPI*, and *ICAM-1* were potently induced by DNA insults in the presence of ectopic TIFA (Fig. 4F). Consistently, ELISA results suggested that the secretion of IL-6 and IL-8 was significantly increased in TIFA-overexpressed cells relative to control cells when they were exposed to ETO (Fig. 4G).

To validate TIFA-induced NF- κ B activation following DNA damage was indeed dependent on IKK pathway, IKK β inhibitor IKK-16 (25) and IKK α inhibitor PS-1145 (26) were used. As shown in Figure 4H, TIFA-induced I κ B α phosphorylation and degradation of total I κ B α upon genotoxic stress were impaired by either IKK-16 or PS-1145 treatment. Consistently, TIFA-induced up-regulation of CXCL10 and GM-CSF following DNA damage were severely suppressed by PS-1145 (Fig. 4I). Together, these results suggested that TIFA-induced NF- κ B activation under genotoxic stress was dependent on IKK activation.

The necessity of TIFA for DNA damage-induced NF- κ B activation was then determined using RPMI-8226 cell line based loss-of-function model. We transduced RPMI-8226 cells with lentiviral shRNA against TIFA or a non-silence control and the efficiency of TIFA depletion was validated by Western blotting (Fig. 4K, right). Importantly, both I κ B α phosphorylation and up-regulation of CXCL10 were greatly suppressed upon TIFA removal (Fig. 4J and 4K), supporting the essential function of endogenous TIFA in DNA damage-activated NF- κ B cascade.

TIFA/TRAF2 Complex Promotes DNA Damage-Induced NEMO Ubiquitination

We next sought to address the molecular mechanisms underlying TIFA-promoted NF- κ B activation following DDR. NEMO as a regulatory subunit of IKK complex, is the controlling nexus for genotoxic stress-induced NF- κ B activation (3,6), we therefore determined the differences of NEMO's interaction partners in TIFA-overexpressing cells versus the control cells when ETO was added, by use of affinity purification and mass spectrometry (MS) analysis (Fig. 5A). Surprisingly, overexpression of TIFA resulted in multiple additional bands in NEMO's interactome, and the MS analysis revealed the presence of both ubiquitin and NEMO in these species (Fig. 5A). Given the crucial function of NEMO ubiquitination in NF- κ B activation and DNA damage response (3,6), we then co-transfected cells with FLAG-tagged NEMO and HA-tagged ubiquitin to examine TIFA-enhanced NEMO ubiquitination following genotoxic stress. Immunoprecipitation and Western blotting analysis confirmed that TIFA could prominently enhance NEMO ubiquitination as indicated by multiple HA-linked NEMO bands under DNA damage conditions (Fig. 5B).

Since phosphorylation event was the key switch for TIFA-mediated NF- κ B activation, we then tested the effect of TIFA-T9A mutant on NEMO ubiquitination, which failed to accumulate on damaged chromatin (Fig. 3). In line, this mutant suppressed DNA damage-elicited NEMO ubiquitination, especially its polyubiquitination forms at higher molecular weight, in comparison to the wild-type TIFA (Fig. 5C), highlighting the significance of chromatin-bound TIFA

in NF- κ B activation. This point was further supported by the marginal induction of NEMO ubiquitination by FHA domain-deleted TIFA following ETO treatment (Fig. 5D), in light of the critical involvement of FHA domain to recognize pThr9 for TIFA oligomerization in NF- κ B activation (13,14,23). Interestingly, with the use of the nuclear lysate prepared from ETO-treated cells, we found the cells transfected with TIFA-T9A mutant showed decreased DNA damage-elicited NEMO ubiquitination, especially its polyubiquitination forms at higher molecular weight, in comparison to the result from wild-type TIFA transfected cells, while the ubiquitination pattern of cytoplasmic NEMO was nearly unaffected (Fig. 5E). Given the critical function of NEMO ubiquitination for DNA damage-induced NF- κ B activation, this result suggested that the nucleus translocation of TIFA for its enrichment on damaged chromatin and the possible intermolecular association between FHA and pThr9 for TIFA oligomerization around DNA damage sites could enhance the efficiency of NEMO ubiquitination upon genotoxic stress.

Further, TIFA-containing protein complexes were affinity purified from extracts of HeLa cells stably expressing FLAG-tagged TIFA under control or DNA damage conditions. These protein complexes were then resolved on SDS-PAGE and silver stained (Fig. 6A). As reported in other canonical NF- κ B pathways, MS analysis identified TRAF2 as the major interacting partner for TIFA following ETO treatment (Fig. 6A). TRAF2 could act as a RING finger type E3 ubiquitin ligase (27), we thus speculated that TRAF2 might be involved in NEMO ubiquitination in TIFA-mediated NF- κ B

activation responding to genotoxic stress. Indeed, polyubiquitination of NEMO was enhanced when TIFA and TRAF2 were overexpressed simultaneously in ETO-treated cells (Fig. 6B). Importantly, epistasis analysis indicated that TIFA-enhanced NEMO polyubiquitination at high molecular weight (indicated by brackets in Fig. 6C) was severely inhibited when endogenous TRAF2 was depleted, implying the necessity of TRAF2 in this pathway.

TIFA Overexpression Is Correlated with Decreased Cancer Cell Proliferation

As stated earlier, DNA damage-induced NF- κ B activation constitutes a secretory senescence barrier against tumorigenesis. To test whether TIFA-mediated NF- κ B activation could be translated into a physiologically relevant response in multiple myeloma cells, we first examined the effect of TIFA on cancer cell proliferation and growth. The results in TIFA-negative U266 cells showed that overexpression of TIFA was correlated with decreased cancer cell proliferation in both ETO-treated and non-treated cells, suggesting minute but inherent genomic instability in cancer cells could take advantage of exogenous TIFA to defeat unlimited proliferation (Fig. 7A, left). To connect TIFA-associated phenotypical changes to its translocation to DNA lesions, we compared cell proliferation of wild-type to the T9A-mutated- TIFA overexpressed cancer cells (Fig. 7A, right). The data indicated that the suppression of cancer cell proliferation by TIFA was impaired by its T9A-mutation, implying that TIFA-associated phenotypical changes correlated with its ability to accumulate on damaged chromatin. Flow cytometry analysis further revealed that cancer cell

cycle progression was significantly accelerated in TIFA-depleted RPMI-8226 cells indicated by the decreased G0/G1 phase cells when TIFA was depleted (Fig. 7B). Moreover, the apoptosis analysis suggested that U266 cells transduced with lentiviral TIFA showed increased apoptosis rate compared with cells transduced with empty vector, especially when ETO was added (Fig. 7C).

DISCUSSION

Mounting evidence suggested the DNA damage-induced NF- κ B activation and secretory phenotypes played crucial roles in both carcinogenesis and senescence, and the identification of TIFA as a novel regulator in this pathway added a new bridge linking DNA damage sensing and IKK complex assembly occurred within two separate compartments. This connection is biochemically composed by the TIFA/TRAF2/NEMO trio and initiated by TIFA's accumulation on damaged chromatin. Regarding to the subcellular localization change of TIFA following genotoxic stress, we proved the significance of TIFA's FHA domain in this process. Our biochemical data suggested that TIFA could interact with γ H2AX-containing nucleosomes; however, *in vitro* pull-down did not support the direct association between TIFA and the C-terminal peptide of H2AX phosphorylated at serine 139 (data not shown). This observation was consistent with the binding preference of FHA domain for phosphorylated threonine over phosphorylated serine (11,12,28). Indeed, we found threonine 9 of TIFA was phosphorylated in response to DNA insults, and the FHA-pThr interaction was crucial for TIFA-mediated NF- κ B activation in genotoxic conditions as its roles in other inflammatory pathways (14,23,29). Benefits

of chromatin enrichment of TIFA for NF- κ B activation could be easily grasped with the fact that oligomerization is a prevailing mechanism for ubiquitination based efficient assembly of IKK complex (4,5). Even in the canonical inflammation signaling pathways, intermolecular binding between FHA and pThr9 was the key event for TIFA oligomerization and downstream TRAFs oligomerization and I κ B phosphorylation (13,14,23). On the other hand, the magnitude of DNA damages could be translated into the amounts of active centers for TIFA association, thus more DNA damage would cause more TIFA concentration and oligomerization to engage stronger NEMO ubiquitination. Since K63-linked polyubiquitination was the key signaling molecules catalyzed by TRAF family E3s (5), the interesting junction that UBC13, as the key E2-conjugating enzyme for K63-linked ubiquitin-chain formation, was also involved in DNA damage response (30-32), suggested that the great availability of UBC13 surrounding DNA damage sites would facilitate nuclear TIFA/TRAF2-mediated NEMO polyubiquitination.

Another interesting finding from this study was the common Thr9 phosphorylation events for both canonical inflammation and DNA damage signaling pathways, despite that different kinases might be involved (29,33). Although the whole picture for the differences of these cascades was currently unknown, nucleus translocation and chromatin enrichment of TIFA could only be observed in DNA damage conditions, but not in inflammatory cascades, suggested that additional regulations exist to account for DNA damage-induced subcellular translocation.

DNA damage-induced secretory phenotype is a crucial component in senescence barrier model for carcinogenesis, and our data suggested that TIFA-mediated NF- κ B activation and secretion responding to genotoxic stress played an inhibitory role for proliferation of multiple myeloma cells. Of note, overexpression of TIFA dramatically augmented transcription of CXCL10, which could attenuate cell proliferation in the presence of IL-6 and eliminate precancerous cells by stimulating immune responses *in vivo* (34,35). Hence, the identification of TIFA/TRAF2 complex as novel molecular targets with regulatory roles in DNA damage-elicited signaling pathways would benefit the development of intervention strategy for carcinogenesis.

EXPERIMENTAL PROCEDURES

Cell culture

HeLa and HEK293T cell lines were maintained by our lab. RPMI-8226 cell lines were purchased from China Infrastructure of Cell Line Resources (Beijing, China). U266 cell lines were kindly provided by Dr. Qing Ge (Peking university health science center, China). HeLa and HEK293T cell lines were cultured in Dulbecco's Modified Eagle Medium (DMEM) supplemented with 10% fetal bovine serum (FBS). RPMI-8226 and U266 cell lines were cultured in RPMI-1640 medium supplemented with 10% FBS. Etoposide (ETO, 40 μ M) was purchased from Sigma (E1383). IKK-16 and PS-1145 were purchased from Selleck.

Western blotting and antibodies

Western blotting analysis was performed according to procedures previously described (19). Western blotting analysis was generally performed for 3-4 times, with a representative blot shown in final figures. The anti-TIFA antibody was raised in rabbit

immunized with synthetic C-terminal peptide (CSSQSSSPTEMDENES) from human TIFA protein. The whole serum was collected after six rounds of immunization, and the final antibody was recovered through affinity purification by use of TIFA C-terminal peptide conjugated resin. Other antibodies used in this study are anti-FLAG (Sigma, F3165), anti-GAPDH (Santa Cruz, sc-47724), anti-Tubulin (Santa Cruz, sc-8035), anti-GFP (Santa Cruz, sc-9996), anti-NEMO (Santa Cruz, sc-8330), anti-TRAF2 (Cell Signaling Technology Inc, 4724), anti-Phospho-I κ B α (Ser32/36) (Cell Signaling Technology Inc, 9246), anti-I κ B α (Cell Signaling Technology Inc, 9242), anti-Phospho-IKK α/β (Ser176/180) (Cell Signaling Technology Inc, 2697), anti-HA (Cell Signaling Technology Inc, 3724), anti-H3 (abgent, AM8433), anti- γ H2AX (Cell Signaling Technology Inc, 9718; Millipore, 05-636), anti- Phospho-Threonine (Cell Signaling Technology Inc, 9381).

Plasmids, siRNAs, and lentiviral transfections

The template DNA of TIFA was a gift from Dr. Ming-Daw Tsai. Human TIFA was cloned into the pcDNA3.1MycHis vector, EGFP-N1 vector, pHLV vector respectively. FLAG-tagged TIFA was subcloned into pcDNA3.1MycHis vector. The FHA domain mutation and T9A mutation of TIFA were generated by PCR and cloned into pcDNA3.1MycHis vector. pNF- κ B-luc, TRAF2 and HA-tagged ubiquitin were maintained by our lab. The template DNA of NEMO was kindly provided by Dr. Tom Gilmore and FLAG-tagged NEMO was subcloned into pcDNA3.1MycHis vector.

siRNAs against TRAF2 and TIFA were purchased from Genepharma (Shanghai,

China). The sequence of TRAF2 siRNA oligonucleotides was 5'-AGAGGCCAGUCAACGACAU-3'. The sequence of TIFA siRNA oligonucleotides was 5'-GGCCGAAAUCCAACAUCU-3'. Cells transfected with plasmids using Lipofectamine 2000 (Invitrogen) were collected after 48 h of incubation. Cells transfected with RNA oligonucleotides using Lipofectamine RNAiMAX (Invitrogen) were collected after 72 h of incubation.

Lentivirus used for knockdown of TIFA in RPMI-8226 cells was purchased from Genepharma (Shanghai, China). According to the manufacturer's instructions, stable transfection was conducted. Briefly, cells with optimal confluency were infected with lentivirus twice in the presence of 5 μ g/ml polybrene and selected for stable cell line with puromycin.

RNA isolation and primers for quantitative RT-PCR

Total RNA was isolated using RNeasy Mini kit (Qiagen) according to the manufacturer's instructions. First strand cDNA was synthesized using RevertAid First Strand cDNA Synthesis Kit (ThermoFisher) following manufacturer's protocol. The relative quantification was calculated using the $\Delta\Delta$ Ct method and normalized to the vector control group with no treatment (NT). The primers used for quantitative RT-PCR were listed below: *IL-6*, forward 5'-TACCCCCAGGAGAAGATTCC-3', reverse 5'-TTTTCTGCCAGTGCCTCTTT-3'; *IL-8*, forward 5'-TAGCAAATTGAGGCCAAGG-3', reverse 5'-AAACCAAGGCACAGTGGAAC-3'; *A20*, forward

5'-AATCCGAGCTGTTCCACTTG-3', reverse 5'-TGGACGGGGATTTCTATCAC-3'; *IL-11*, forward 5'-ACATGAACTGTGTTTGCCGC-3', reverse 5'-AGCTGGGAATTTGTCCTCAG-3'; *CCL5*, forward 5'-CTGCTGCTTTGCCTACATTG-3', reverse 5'-ACACACTTGGCGGTTCTTTC-3'; *GM-CSF*, forward 5'-ATGTGAATGCCATCCAGGAG-3', reverse 5'-AGGGCAGTGCTGCTTGTAGT-3'; *CXCL3*, forward 5'-GCAGGGAATTCACCTCAAGA-3', reverse 5'-GGTGCTCCCCTTGTTTCAGTA-3'; *MCPI*, forward 5'-CCCCAGTCACCTGCTGTTAT-3', reverse 5'-TGGAATCCTGAACCCACTTC-3'; *ICAM-1*, forward 5'-GGCTGGAGCTGTTTGAGAAC-3', reverse 5'-ACTGTGGGGTTCAACCTCTG-3'; *CXCL10*, forward 5'-CCACGTGTTGAGATCATTGC-3', reverse 5'-CTTGATGGCCTTCGATTCTG-3'; *GAPDH*, forward 5'-CGACCACTTTGTCAAGCTCA-3', reverse 5'-AGGGGTCTACATGGCAACTG-3'.

Luciferase activity assay

All plasmids used in luciferase activity assay were transfected using Lipofectamine 2000 (Invitrogen). Cells were collected after 24 h transfection and cell lysates were prepared with the Dual Luciferase reporter assay kit (Promega) following manufacturer's instructions. Reporter

plasmid was transfected together with renilla plasmid used for normalizing of transfection.

Chromatin fractionation

Chromatin fractionation was performed as previously described with modification (36). In brief, about 5×10^7 cells were collected and washed with ice cold PBS. Then cell pellets were resuspended in 500 μ l of buffer A (10 mM HEPES, pH7.9, 10 mM KCl, 1.5 mM MgCl₂, 0.34 M sucrose, 10% glycerol, 1 mM DTT, 0.05% Triton X-100, PMSF and phosphatase inhibitor cocktail) followed by incubation on ice for 5 min. Then samples were centrifugated at 14,000 rpm for 5 min, 4°C. The pellets were washed once with 500 μ l of buffer A at 14,000 rpm for 5 min. Then the pellets were resuspended in 500 μ l of buffer B (3 mM EDTA, 0.2 mM EGTA, 1 mM DTT, PMSF and phosphatase inhibitor cocktail) followed by incubation on ice for 10 min. Then samples were centrifugated at 2,000 rpm for 5 min, 4°C. The pellets were washed once with 500 μ l of buffer B at 14,000 rpm for 1 min. Finally, the final chromatin fraction were collected. For Western blotting analysis, the chromatin pellets were resuspended in 200 μ l of 2 \times SDS sample buffer and sonicated for 15 s. Chromatin fractionation using nuclear lysis buffer containing 150 mM KOAc was performed as previously described with little modification (22). Cells were incubated in cytoplasmic lysis buffer (10 mM Tris-HCl, pH 7.9, 0.34 M sucrose, 3 mM CaCl₂, 2 mM MgOAc, 0.1 mM EDTA, 1 mM dithiothreitol, 0.5% Nonidet P-40 and protease inhibitors) for 10 min on ice. Then cell lysis were centrifugated at 3500 g for

15 min. Supernants were collected. Nuclei pellets were further lysed in nuclear lysis buffer (20 mM HEPES, pH 7.9, 3 mM EDTA, 10% glycerol, 150 mM KOAc, 1.5 mM MgCl₂, 1 mM dithiothreitol, 0.1% Nonidet P-40 and protease inhibitors) for 10 min on ice. Then cell lysis were centrifugated at 10,000 g for 30 min. Supernants were collected. The chromatin-enriched pellet was resuspended in 200 μ l of 2 \times SDS sample buffer and sonicated for 15 s.

Growth curve assay

Growth curve was determined by Cell Counting Kit-8 (CCK-8) (Vazyme) and performed according to the manufacturer's protocol. In brief, cells were seeded in 96-well plates at a density of 2×10^3 per well. 10 μ l of CCK-8 reagent was added each well and incubated for 2 h. Following shaking, the absorbance at 450 nm was measured. The absorbance was measured at 0, 1, 2, 3, 4 and 5 days after plating.

Flow Cytometry Assay

For cell cycle analysis, suspended cells were collected by centrifugation and then washed with cold PBS. Then cells were fixed with 70% ethanol overnight at 4°C and RNase A (Sigma) was added at 37°C for 30 min for RNA digestion. After which, propidium iodide (PI) (Millipore) was used for staining. BD FACS flow cytometer was used for analysis of DNA content. For apoptosis analysis, samples were prepared according to the manufacturer's instructions (KeyGEN BioTECH). Briefly, cells were stained with Annexin V and PI, after which, BD FACS flow cytometer was used for analysis of apoptosis.

Acknowledgments: This work was supported by grants from the National Natural Science Foundation of China, No. 81771495, 81300254 and 81372164 and the National Basic Research Programs of China, No. 2013CB530801.

Conflict of interest: The authors declare that they have no conflicts of interest with the contents of this article.

REFERENCES

1. Lopez-Otin, C., Blasco, M. A., Partridge, L., Serrano, M., and Kroemer, G. (2013) The hallmarks of aging. *Cell* **153**, 1194-1217
2. Coppe, J. P., Patil, C. K., Rodier, F., Sun, Y., Munoz, D. P., Goldstein, J., Nelson, P. S., Desprez, P. Y., and Campisi, J. (2008) Senescence-associated secretory phenotypes reveal cell-nonautonomous functions of oncogenic RAS and the p53 tumor suppressor. *PLoS Biol.* **6**, 2853-2868
3. McCool, K. W., and Miyamoto, S. (2012) DNA damage-dependent NF-kappaB activation: NEMO turns nuclear signaling inside out. *Immunological reviews* **246**, 311-326
4. Hayden, M. S., and Ghosh, S. (2008) Shared principles in NF-kappaB signaling. *Cell* **132**, 344-362
5. Chen, Z. J. (2005) Ubiquitin signalling in the NF-kappaB pathway. *Nat. Cell Biol.* **7**, 758-765
6. Miyamoto, S. (2011) Nuclear initiated NF-kappaB signaling: NEMO and ATM take center stage. *Cell research* **21**, 116-130
7. Huang, T. T., Wuerzberger-Davis, S. M., Wu, Z. H., and Miyamoto, S. (2003) Sequential modification of NEMO/IKKgamma by SUMO-1 and ubiquitin mediates NF-kappaB activation by genotoxic stress. *Cell* **115**, 565-576
8. Wu, Z. H., Shi, Y., Tibbetts, R. S., and Miyamoto, S. (2006) Molecular linkage between the kinase ATM and NF-kappaB signaling in response to genotoxic stimuli. *Science* **311**, 1141-1146
9. Kanamori, M., Suzuki, H., Saito, R., Muramatsu, M., and Hayashizaki, Y. (2002) T2BP, a novel TRAF2 binding protein, can activate NF-kappaB and AP-1 without TNF stimulation. *Biochemical and biophysical research communications* **290**, 1108-1113
10. Takatsuna, H., Kato, H., Gohda, J., Akiyama, T., Moriya, A., Okamoto, Y., Yamagata, Y., Otsuka, M., Umezawa, K., Semba, K., and Inoue, J. (2003) Identification of TIFA as an adapter protein that links tumor necrosis factor receptor-associated factor 6 (TRAF6) to interleukin-1 (IL-1) receptor-associated kinase-1 (IRAK-1) in IL-1 receptor signaling. *J. Biol. Chem.* **278**, 12144-12150
11. Pennell, S., Westcott, S., Ortiz-Lombardia, M., Patel, D., Li, J., Nott, T. J., Mohammed, D., Buxton, R. S., Yaffe, M. B., Verma, C., and Smerdon, S. J. (2010) Structural and functional analysis of phosphothreonine-dependent FHA domain interactions. *Structure* **18**, 1587-1595
12. Reinhardt, H. C., and Yaffe, M. B. (2013) Phospho-Ser/Thr-binding domains: navigating the cell cycle and DNA damage response. *Nat. Rev. Mol. Cell Biol.* **14**,

563-580

13. Ea, C. K., Sun, L., Inoue, J., and Chen, Z. J. (2004) TIFA activates IkappaB kinase (IKK) by promoting oligomerization and ubiquitination of TRAF6. *Proc. Natl. Acad. Sci. U. S. A.* **101**, 15318-15323
14. Huang, C. C., Weng, J. H., Wei, T. Y., Wu, P. Y., Hsu, P. H., Chen, Y. H., Wang, S. C., Qin, D., Hung, C. C., Chen, S. T., Wang, A. H., Shyy, J. Y., and Tsai, M. D. (2012) Intermolecular binding between TIFA-FHA and TIFA-pT mediates tumor necrosis factor alpha stimulation and NF-kappaB activation. *Mol. Cell. Biol.* **32**, 2664-2673
15. Li, Q., Zhang, Y., Fu, J., Han, L., Xue, L., Lv, C., Wang, P., Li, G., and Tong, T. (2013) FOXA1 mediates p16(INK4a) activation during cellular senescence. *The EMBO journal* **32**, 858-873
16. Zhang, Y., Zhang, D., Li, Q., Liang, J., Sun, L., Yi, X., Chen, Z., Yan, R., Xie, G., Li, W., Liu, S., Xu, B., Li, L., Yang, J., He, L., and Shang, Y. (2016) Nucleation of DNA repair factors by FOXA1 links DNA demethylation to transcriptional pioneering. *Nature genetics* **48**, 1003-1013
17. Zhang, Y., Yang, X., Gui, B., Xie, G., Zhang, D., Shang, Y., and Liang, J. (2011) Corepressor protein CDYL functions as a molecular bridge between polycomb repressor complex 2 and repressive chromatin mark trimethylated histone lysine 27. *J. Biol. Chem.* **286**, 42414-42425
18. Wang, W., Wu, J., Zhang, Z., and Tong, T. (2001) Characterization of regulatory elements on the promoter region of p16(INK4a) that contribute to overexpression of p16 in senescent fibroblasts. *J. Biol. Chem.* **276**, 48655-48661
19. Cao, X., Xue, L., Han, L., Ma, L., Chen, T., and Tong, T. (2011) WW domain-containing E3 ubiquitin protein ligase 1 (WWP1) delays cellular senescence by promoting p27(Kip1) degradation in human diploid fibroblasts. *J. Biol. Chem.* **286**, 33447-33456
20. Chen, T., Xue, L., Niu, J., Ma, L., Li, N., Cao, X., Li, Q., Wang, M., Zhao, W., Li, G., Wang, J., and Tong, T. (2012) The retinoblastoma protein selectively represses E2F1 targets via a TAAC DNA element during cellular senescence. *J. Biol. Chem.* **287**, 37540-37551
21. Zhang, Y., and Tong, T. (2014) FOXA1 antagonizes EZH2-mediated CDKN2A repression in carcinogenesis. *Biochemical and biophysical research communications* **453**, 172-178
22. Zhao, Q., Wang, Q. E., Ray, A., Wani, G., Han, C., Milum, K., and Wani, A. A. (2009) Modulation of nucleotide excision repair by mammalian SWI/SNF chromatin-remodeling complex. *J. Biol. Chem.* **284**, 30424-30432
23. Weng, J. H., Hsieh, Y. C., Huang, C. C., Wei, T. Y., Lim, L. H., Chen, Y. H., Ho, M. R., Wang, I., Huang, K. F., Chen, C. J., and Tsai, M. D. (2015) Uncovering the Mechanism of Forkhead-Associated Domain-Mediated TIFA Oligomerization That Plays a Central Role in Immune Responses. *Biochemistry* **54**, 6219-6229
24. Barretina, J., Caponigro, G., Stransky, N., Venkatesan, K., Margolin, A. A., Kim, S., Wilson, C. J., Lehár, J., Kryukov, G. V., Sonkin, D., Reddy, A., Liu, M., Murray, L., Berger, M. F., Monahan, J. E., Morais, P., Meltzer, J., Korejwa, A., Jane-Valbuena, J.,

- Mapa, F. A., Thibault, J., Bric-Furlong, E., Raman, P., Shipway, A., Engels, I. H., Cheng, J., Yu, G. K., Yu, J., Aspesi, P., Jr., de Silva, M., Jagtap, K., Jones, M. D., Wang, L., Hatton, C., Palesscandolo, E., Gupta, S., Mahan, S., Sougnez, C., Onofrio, R. C., Liefeld, T., MacConaill, L., Winckler, W., Reich, M., Li, N., Mesirov, J. P., Gabriel, S. B., Getz, G., Ardlie, K., Chan, V., Myer, V. E., Weber, B. L., Porter, J., Warmuth, M., Finan, P., Harris, J. L., Meyerson, M., Golub, T. R., Morrissey, M. P., Sellers, W. R., Schlegel, R., and Garraway, L. A. (2012) The Cancer Cell Line Encyclopedia enables predictive modelling of anticancer drug sensitivity. *Nature* **483**, 603-607
25. Duckworth, C., Zhang, L., Carroll, S. L., Ethier, S. P., and Cheung, H. W. (2016) Overexpression of GAB2 in ovarian cancer cells promotes tumor growth and angiogenesis by upregulating chemokine expression. *Oncogene* **35**, 4036-4047
26. Hideshima, T., Chauhan, D., Richardson, P., Mitsiades, C., Mitsiades, N., Hayashi, T., Munshi, N., Dang, L., Castro, A., Palombella, V., Adams, J., and Anderson, K. C. (2002) NF-kappa B as a therapeutic target in multiple myeloma. *J. Biol. Chem.* **277**, 16639-16647
27. Pineda, G., Ea, C. K., and Chen, Z. J. (2007) Ubiquitination and TRAF signaling. *Advances in experimental medicine and biology* **597**, 80-92
28. Durocher, D., Taylor, I. A., Sarbassova, D., Haire, L. F., Westcott, S. L., Jackson, S. P., Smerdon, S. J., and Yaffe, M. B. (2000) The molecular basis of FHA domain:phosphopeptide binding specificity and implications for phospho-dependent signaling mechanisms. *Mol. Cell* **6**, 1169-1182
29. Lin, T. Y., Wei, T. W., Li, S., Wang, S. C., He, M., Martin, M., Zhang, J., Shentu, T. P., Xiao, H., Kang, J., Wang, K. C., Chen, Z., Chien, S., Tsai, M. D., and Shyy, J. Y. (2016) TIFA as a crucial mediator for NLRP3 inflammasome. *Proc. Natl. Acad. Sci. U. S. A.* **113**, 15078-15083
30. Messick, T. E., and Greenberg, R. A. (2009) The ubiquitin landscape at DNA double-strand breaks. *The Journal of cell biology* **187**, 319-326
31. Wang, B., and Elledge, S. J. (2007) Ubc13/Rnf8 ubiquitin ligases control foci formation of the Rap80/Abraxas/Brcal/Brc36 complex in response to DNA damage. *Proc. Natl. Acad. Sci. U. S. A.* **104**, 20759-20763
32. Brusky, J., Zhu, Y., and Xiao, W. (2000) UBC13, a DNA-damage-inducible gene, is a member of the error-free postreplication repair pathway in *Saccharomyces cerevisiae*. *Current genetics* **37**, 168-174
33. Wei, T. W., Wu, P. Y., Wu, T. J., Hou, H. A., Chou, W. C., Teng, C. J., Lin, C. R., Chen, J. M., Lin, T. Y., Su, H. C., Huang, C. F., Yu, C. R., Hsu, S. L., Tien, H. F., and Tsai, M. D. (2017) Aurora A and NF-kappaB Survival Pathway Drive Chemoresistance in Acute Myeloid Leukemia via the TRAF-Interacting Protein TIFA. *Cancer Res.* **77**, 494-508
34. Brownell, J., and Polyak, S. J. (2013) Molecular pathways: hepatitis C virus, CXCL10, and the inflammatory road to liver cancer. *Clin. Cancer Res.* **19**, 1347-1352
35. Barash, U., Zohar, Y., Wildbaum, G., Beider, K., Nagler, A., Karin, N., Ilan, N., and Vlodaysky, I. (2014) Heparanase enhances myeloma progression via CXCL10 downregulation. *Leukemia* **28**, 2178-2187

36. Li, D. Q., Nair, S. S., Ohshiro, K., Kumar, A., Nair, V. S., Pakala, S. B., Reddy, S. D., Gajula, R. P., Eswaran, J., Aravind, L., and Kumar, R. (2012) MORC2 signaling integrates phosphorylation-dependent, ATPase-coupled chromatin remodeling during the DNA damage response. *Cell Rep* **2**, 1657-1669

Footnotes

The abbreviations used are: TRAF-interacting protein with forkhead-associated domain (TIFA), TNF receptor-associated factor 2 (TRAF2), Interleukin (IL), NF- κ B essential modulator (NEMO), Inhibitors of NF- κ B (I κ B).

FIGURE LEGENDS

Figure 1: Enrichment of TIFA on chromatin following DNA damage. (A) Confocal microscopic examination of TIFA and γ H2AX in HeLa cells transfected with FLAG-TIFA were treated with vehicle (Veh) or etoposide (ETO). DAPI was used to visualize the nucleus. Scale bar represents 20 μ m. (B) Chromatin fractions were isolated from the HeLa cells expressing FLAG-TIFA in the absence or presence of ETO. These fractions were then subjected to Western blotting with indicated antibodies. (C) Chromatin fractions were isolated using nuclear lysis buffer containing 150 mM KOAc from HeLa cells expressing FLAG-TIFA in the absence or presence of ETO. The purified chromatin fraction and subcellular fractions were then probed with indicated antibodies. (D) Chromatin fractions were isolated using nuclear lysis buffer containing 150 mM KOAc from HeLa cells expressing FLAG-TIFA in the absence or presence of LPS. The subcellular fractions were then probed with indicated antibodies. (E) Chromatin fractions were isolated using nuclear lysis buffer containing 150 mM KOAc from U266 cells stably expressing TIFA. The subcellular fractions were then probed with indicated antibodies. (F) Chromatin fractions were isolated using nuclear lysis buffer containing 150 mM KOAc from RPMI-8226 cells. The subcellular fractions were then probed with indicated antibodies.

Figure 2: TIFA potentiates DNA damage-induced NF- κ B activation and secretion. (A) NF- κ B luciferase reporter was transfected to HeLa cells stably expressing FLAG-TIFA or control cells. Renilla vector was also transfected simultaneously served as transfection control. After treatment of cells with ETO with indicated times, the cells were harvested for luciferase activity assay. Data were represented as the means \pm standard deviation (SD) from three independent experiments. $**P < 0.01$ (Student's *t*-test). (B) The HeLa cells were transfected with control or FLAG-TIFA expression vectors. After two days, the cells were further treated with vehicle or ETO for 6h. The cell lysate was then harvested for Western blotting analysis with indicated antibodies. p-I κ B α indicates the antibody against I κ B α phosphorylation on serine 32 and serine 36. (C) The total mRNA was prepared from cells described in (B) and the mRNA levels of indicated genes were examined using quantitative RT-PCR analysis. Data were represented as the means \pm standard deviation (SD) from eight independent experiments. $**P < 0.01$ (Student's *t*-test). (D) The HeLa cells were transfected with control or FLAG-TIFA expression vectors and further treated with or without ETO. The secretory levels of IL-6 and IL-8 were then measured by ELISA. Data were represented as the means

\pm standard deviation (SD) from three independent experiments. $**P < 0.01$ (Student's *t*-test).

Figure 3: The significance of phosphorylation event in TIFA-mediated NF- κ B activation.

(A) The vectors expressing full-length TIFA, the FHA domain (TIFA FHA), the R51A/K88A/N89A (MT1), or the G50E/S66A (MT2) mutants of full-length TIFA were transfected in HeLa cells with no treatment (NT) or treatment of ETO. The mRNA levels of indicated genes were examined using quantitative RT-PCR analysis. Data were represented as the means \pm standard deviation (SD) from eight independent experiments. $**P < 0.01$ (Student's *t*-test). (B) The lysates of TIFA-stably expressed HeLa cells with no treatment (NT) or treatment of ETO were subjected to immunoprecipitation using FLAG antibody and probed with indicated antibodies. Before harvesting cells, cells were treated with formaldehyde for 10 min. (C) FLAG-TIFA was co-transfected with wild-type H2AX (WT), non-phosphorylatable mutant S139A of H2AX (SA) or phosphorylation mimicking mutant S139E of H2AX (SE) in HeLa cells. Cells described were treated with ETO or LPS and the mRNA levels of indicated genes were examined using quantitative RT-PCR analysis. Data were represented as the means \pm standard deviation (SD) from six independent experiments. $**P < 0.01$ (Student's *t*-test). (D) Whole cell lysates and chromatin fractions from HeLa cells expressing TIFA or T9A mutant upon damage treatment were subjected to Western blotting analysis probed with indicated antibodies. (E) Whole cell lysates from HeLa cells expressing vector, TIFA and T9A mutant upon damage treatment were subjected to Western blotting analysis probed with indicated antibodies. (F) The total mRNA was prepared from cells described in (E) and the mRNA levels of indicated genes were examined using quantitative RT-PCR analysis. Data were represented as the means \pm standard deviation (SD) from three independent experiments. $**P < 0.01$ (Student's *t*-test). (G) Cells were transfected with FLAG-tagged TIFA or T9A mutant as indicated with or without DNA damage treatment. Cellular extracts were prepared and immunoprecipitation was performed with FLAG antibody. IgG light chain is indicated with *.

Figure 4: TIFA potentiates DNA damage-induced NF- κ B activation in myeloma cells.

(A) The dataset of TIFA mRNA expression levels across ~1000 cell lines were retrieved from the Cancer Cell Line Encyclopedia (CCLE). The sorted data was log transformed and the haematopoietic or lymphoid cells were highlighted in red. (B) The whole cell lysates from indicated cell lines were subjected to Western blotting analysis with anti-TIFA antibody to assess its endogenous protein levels. (C) Time-course measurement of protein levels in U266 cells infected with lentivirus expressing TIFA (pHBLV-TIFA) or control (pHBLV) and treated with ETO. (D) The U266 cells infected with lentivirus expressing TIFA (pHBLV-TIFA) or control (pHBLV) were treated with ETO as indicated. The cell lysate was then harvested for Western blotting analysis with indicated antibodies. (E) The U266 cells were infected with lentivirus expressing TIFA (pHBLV-TIFA) or control (pHBLV) and then treated with ETO for 2 h or 6 h. The mRNA levels of indicated genes were examined using quantitative RT-PCR analysis. Data were represented as the means \pm standard deviation (SD) from three independent experiments. $**P < 0.01$ (Student's *t*-test). (F) The U266 cells were infected with lentivirus expressing TIFA (pHBLV-TIFA) or control (pHBLV) and then treated with ETO for

2 h or 6 h. The mRNA levels of indicated genes were examined using quantitative RT-PCR analysis. Data were represented as the means \pm standard deviation (SD) from eight independent experiments. * P < 0.05, ** P < 0.01 (Student's t -test). (G) U266 cells infected with lentivirus expressing TIFA (pHBLV-TIFA) or control (pHBLV) were further treated with or without ETO. The secretory levels of IL-6 and IL-8 were then measured by ELISA. Data were represented as the means \pm standard deviation (SD) from three independent experiments. ** P < 0.01 (Student's t -test). (H and I) U266 cells infected with lentivirus expressing TIFA (pHBLV-TIFA) or control (pHBLV) were further treated with ETO and IKK inhibitors IKK-16 or PS-1145. The whole cell lysate and mRNA from cells described above were then prepared for Western blotting analysis or quantitative RT-PCR analysis. Data of quantitative RT-PCR analysis were represented as the means \pm standard deviation (SD) from three independent experiments. * P < 0.05, ** P < 0.01 (Student's t -test). (J) RPMI-8226 cells infected with shRNA control or shRNA against TIFA using lentivirus were further treated with ETO for 2 h or 6 h. Western blotting analysis was then performed to examine the expression levels of indicated proteins. (K) The total mRNA was prepared from cells described in (J) and the mRNA levels of indicated gene was examined using quantitative RT-PCR analysis. Data were represented as the means \pm standard deviation (SD) from three independent experiments. ** P < 0.01 (Student's t -test). The right panel showed knockdown efficiency of TIFA protein.

Figure 5: TIFA promotes DNA damage-induced NEMO ubiquitination. (A) FLAG-NEMO was co-transfected with control vector or EGFP-TIFA to HeLa cells. Cellular extracts were immunopurified with FLAG M2 resin and eluted with FLAG peptide. Eluted proteins were resolved by SDS-PAGE and silver stained. The bands were retrieved and analyzed by mass spectrometry. (B) HeLa cells were co-transfected with FLAG-NEMO, HA-Ub and EGFP-TIFA as indicated. All the cells were treated with ETO before cellular extracts prepared. The immunoprecipitation was performed with FLAG antibody and the immunoprecipitated proteins were examined with indicated antibody. (C) HeLa cells were transfected with plasmids expressing wild-type TIFA or its T9A mutant (TIFA T9A) together with other indicated constructions. The immunoprecipitation assay was performed as in (B). IgG heavy chain is indicated with *. (D) HeLa cells were transfected with plasmids expressing wild-type TIFA or its FHA domain deleted mutant (TIFA Δ FHA) together with other indicated constructions. The immunoprecipitation assay was performed as in (B). IgG heavy chain is indicated with *. (E) HeLa cells were transfected with plasmids expressing wild-type TIFA or its T9A mutant (TIFA T9A) together with other indicated constructions. The cells were harvested and then plasma and nucleus was isolated. The immunoprecipitation assay was performed.

Figure 6: The critical function of TRAF2 in TIFA-mediated NEMO ubiquitination. (A) The extracts from cells stably expressing control vector or FLAG-TIFA in the absence or presence of ETO were immunoprecipitated with FLAG M2 resin and eluted with FLAG peptide. Silver stain and mass spectrometric analysis were performed as in Figure 5A. (B) The HeLa cells were co-transfected with FLAG-NEMO, HA-Ub, EGFP-TIFA and TRAF2 as indicated. All the cells were treated with ETO before cellular extracts prepared. The

immunoprecipitation was performed with FLAG antibody and the immunoprecipitated proteins were examined with HA antibody. (C) The HeLa cells transfected with indicated plasmids were further co-transfected with siRNA control or siRNA targeting TRAF2. All the cells were treated with ETO before cellular extracts prepared. The immunoprecipitation was performed as in (B).

Figure 7: TIFA overexpression is correlated with decreased cancer cell proliferation. (A) Growth curves of U266 cells infected with lentivirus expressing TIFA (pHBLV-TIFA) or control (pHBLV) in the absence or presence of ETO were determined by CCK-8 (left). Growth curves of U266 cells infected with lentivirus expressing TIFA (pHBLV-TIFA), TIFA-T9A (pHBLV-TIFA-T9A) or control (pHBLV) in the presence of ETO were determined by CCK-8 (right). Data were represented as the means \pm standard deviation (SD) from three independent experiments. # $P < 0.05$, TIFA vs. Vector. * $P < 0.05$, TIFA vs. Vector in the presence of ETO. ** $P < 0.05$, TIFA vs. TIFA-T9A. (B) The RPMI-8226 cells infected with lentivirus expressing shRNA control or shRNA against TIFA were further treated with vehicle or ETO. The flow cytometry was then used to evaluate the effect of TIFA on cell cycle progression. (C) The U266 cells infected with lentivirus expressing TIFA (pHBLV-TIFA) or the control (pHBLV) were further treated with vehicle or ETO. The cells were then subjected to apoptosis analysis using PI and Annexin-V double staining method. The portion of apoptotic cells (the upper right and bottom right quadrants) was indicated.

Figure 1

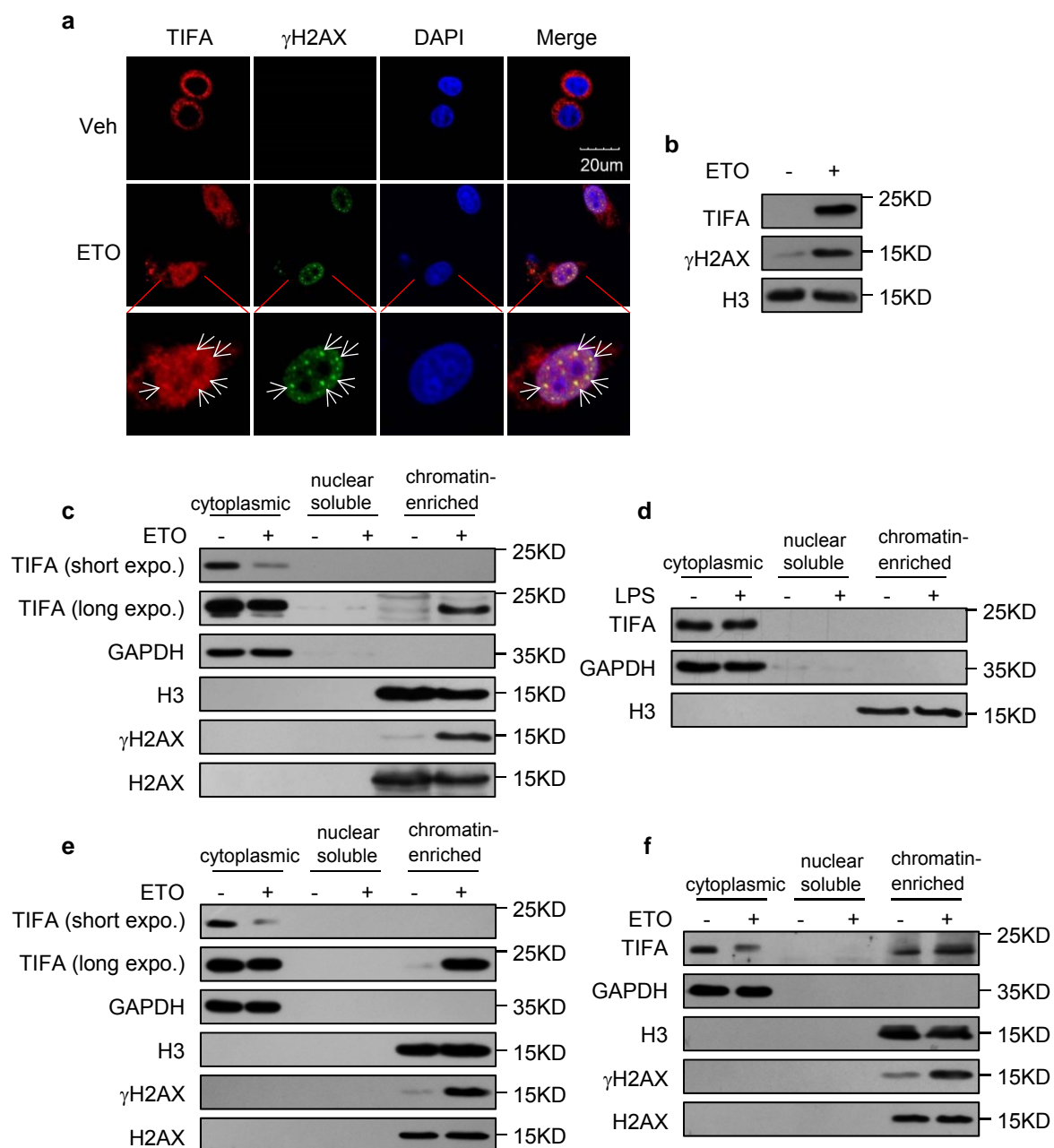


Figure 2

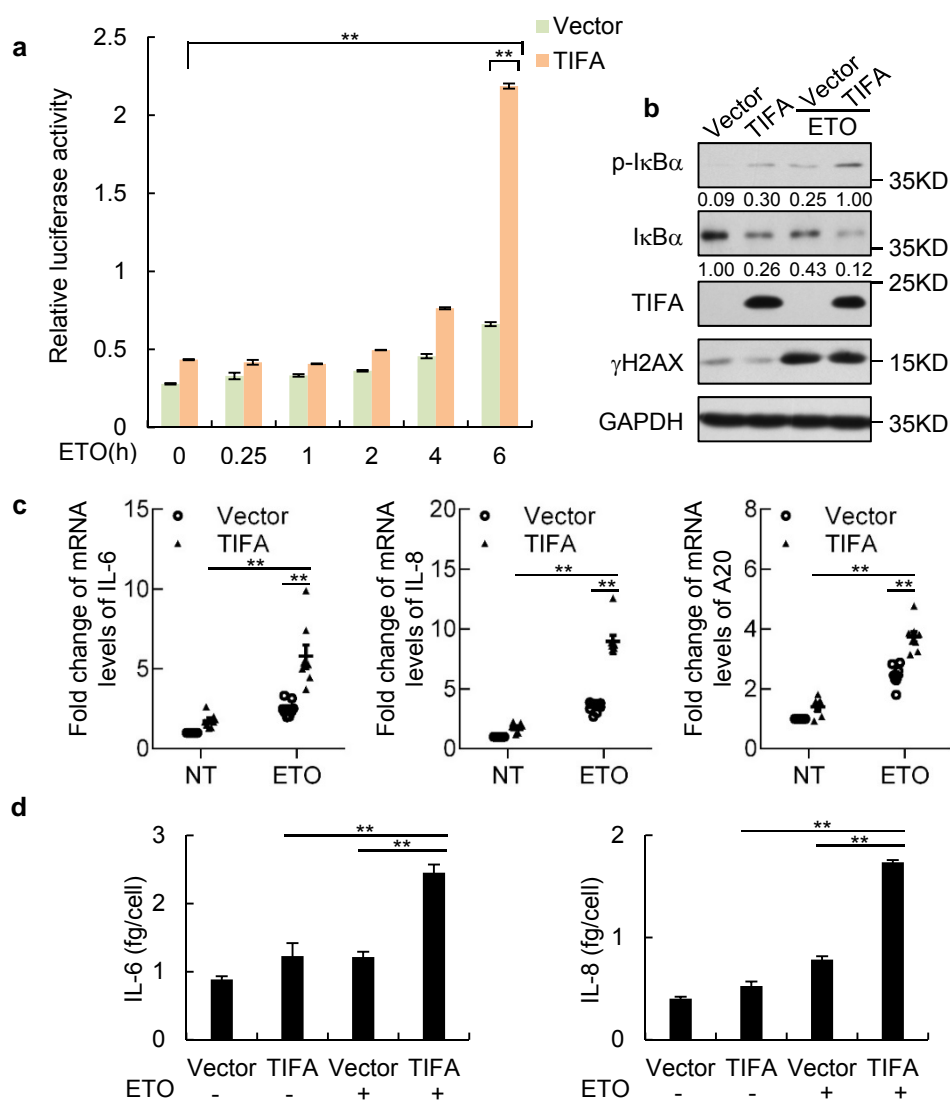


Figure 3

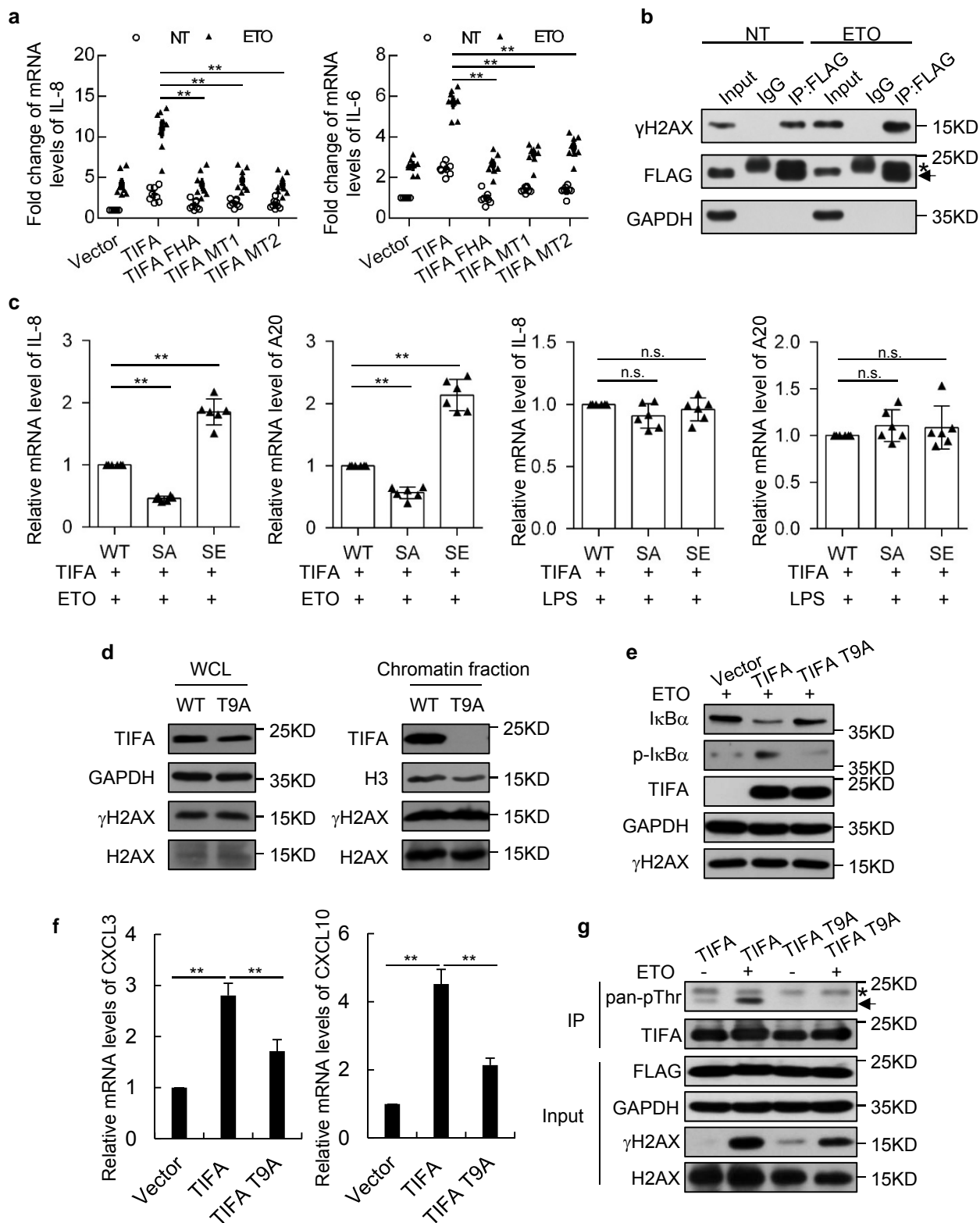


Figure 4

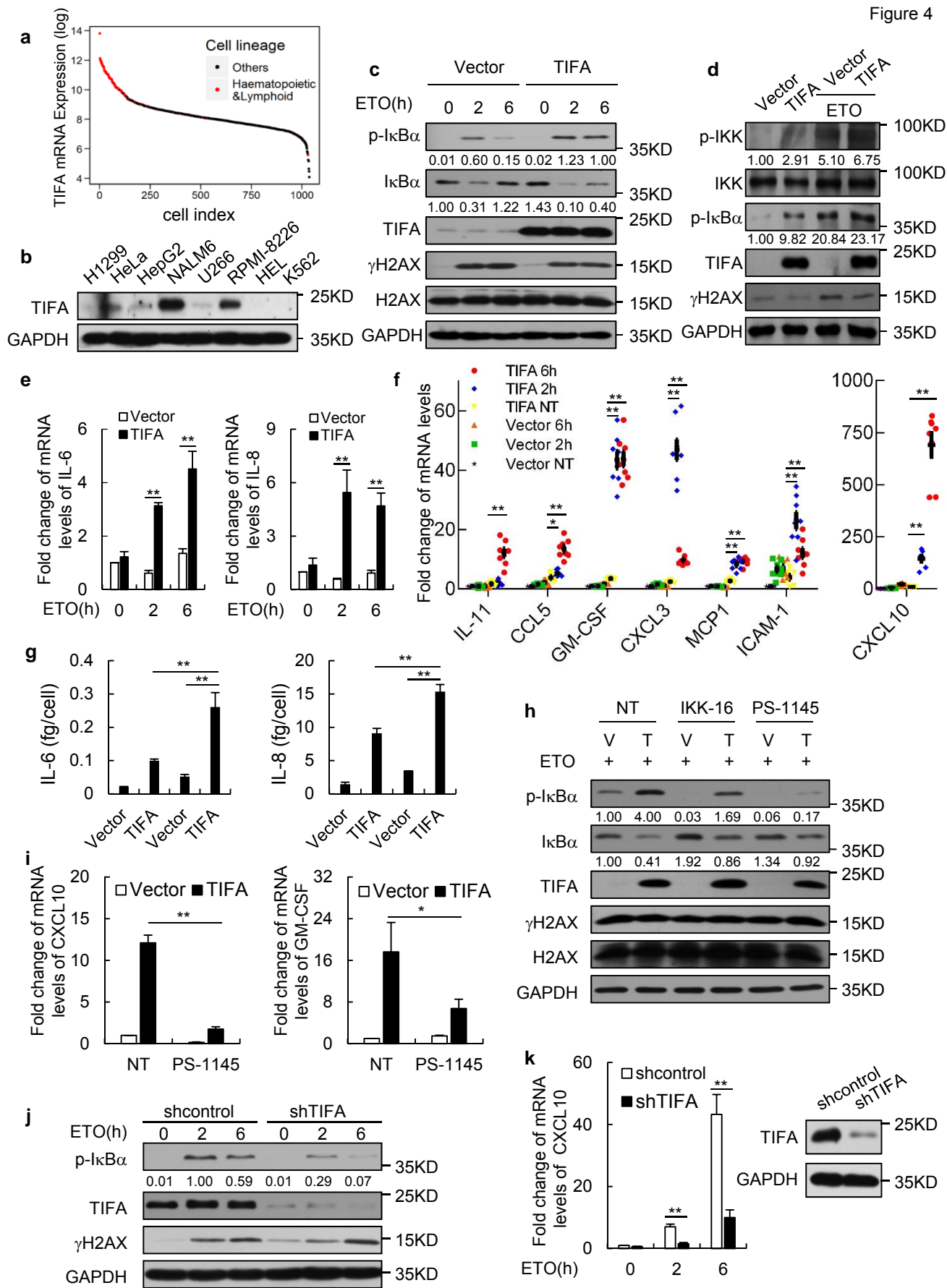


Figure 5

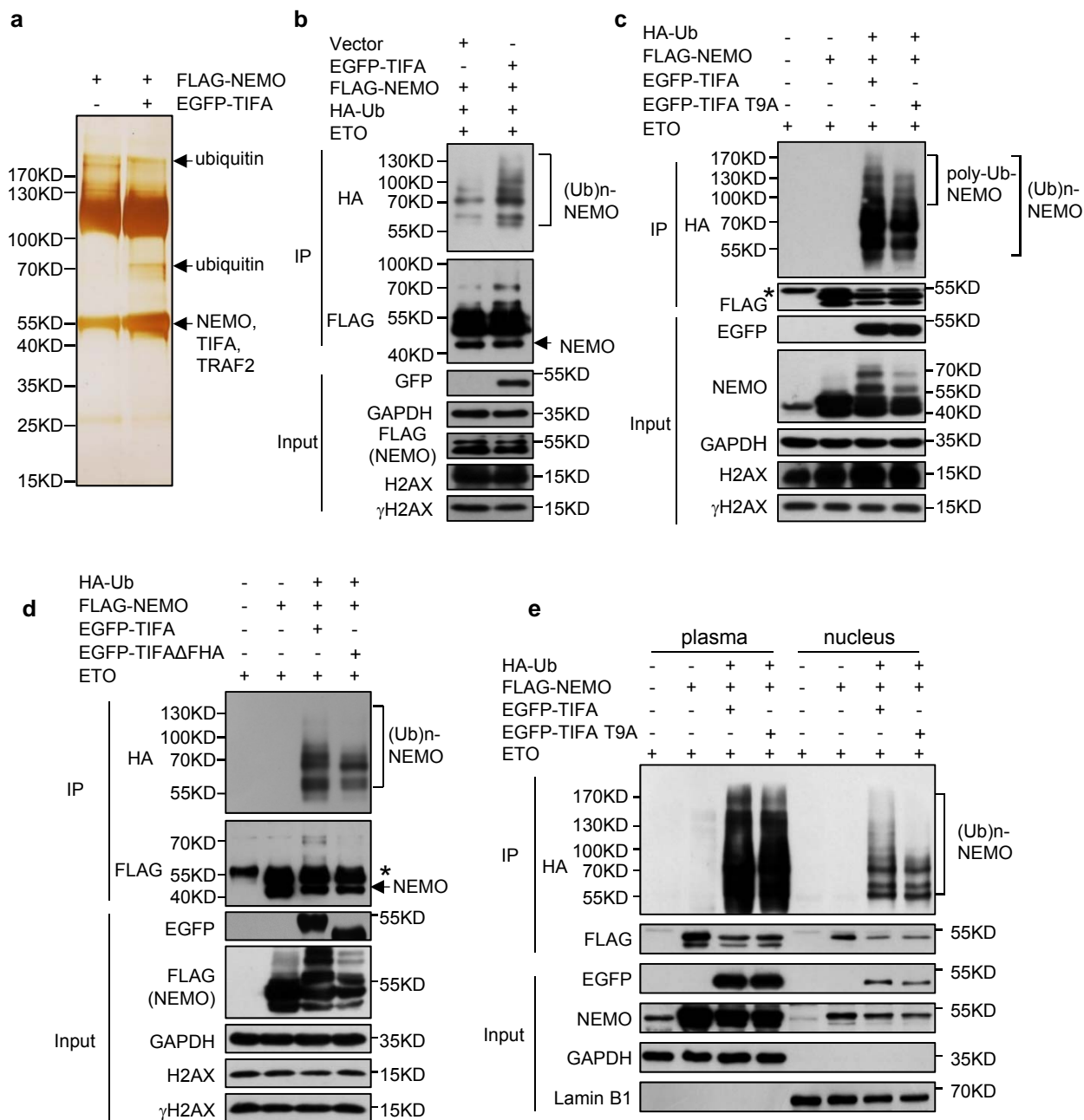


Figure 6

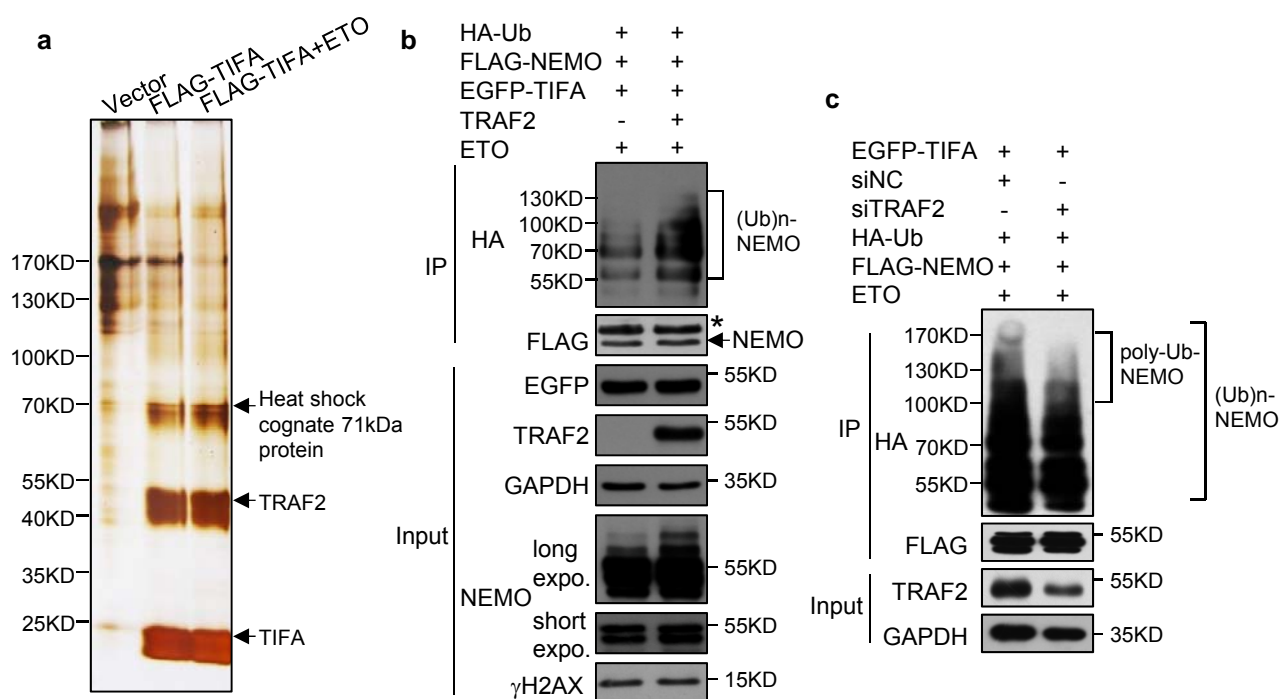
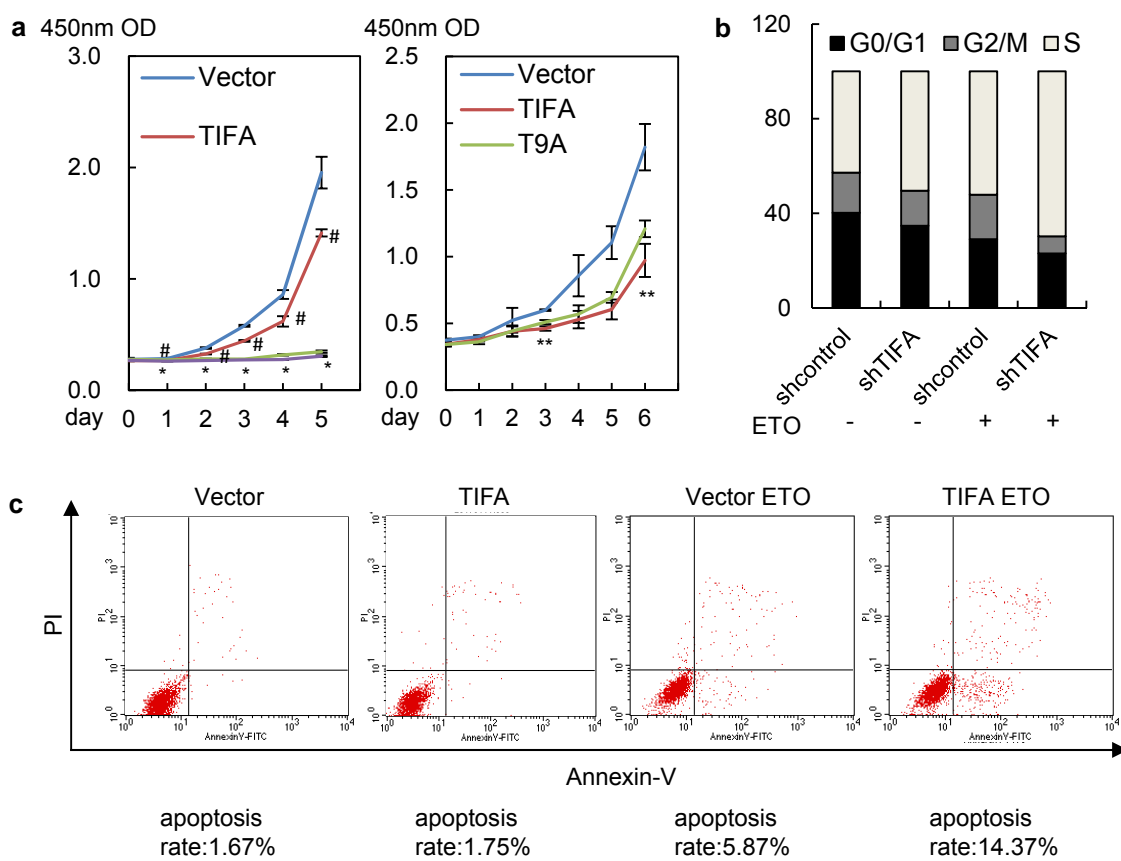


Figure 7



**TRAF-interacting protein with forkhead-associated domain (TIFA) transduces
DNA damage–induced activation of NF- κ B**
Jingxuan Fu, Daoyuan Huang, Fuwen Yuan, Nan Xie, Qian Li, Xinpei Sun, Xuehong
Zhou, Guodong Li, Tanjun Tong and Yu Zhang

J. Biol. Chem. published online March 26, 2018

Access the most updated version of this article at doi: [10.1074/jbc.RA117.001684](https://doi.org/10.1074/jbc.RA117.001684)

Alerts:

- [When this article is cited](#)
- [When a correction for this article is posted](#)

[Click here](#) to choose from all of JBC's e-mail alerts